

Supplementary Information

**High-efficiency catalytic reduction of residual oxygen for purification of carbon dioxide streams from high-pressure oxy-combustion systems**

Hong Lu,<sup>a</sup> Luke Schideman,<sup>ab</sup> Qing Ye<sup>a</sup> and Yongqi Lu<sup>\*a</sup>

<sup>a</sup> Illinois State Geological Survey, University of Illinois at Urbana-Champaign, 615 E. Peabody Drive, Champaign, Illinois, 61801, United States

<sup>b</sup> Departmental of Chemical & Biomolecular Engineering, University of Illinois at Urbana-Champaign, 600 S. Matthews Avenue, Urbana, Illinois, 61801, United States

\* Corresponding Author: E-mail: [yongqilu@illinois.edu](mailto:yongqilu@illinois.edu) (Yongqi Lu)

## Contents

Table S1 XRD peak shifts for  $\text{Co}_{40}\text{Mn}_1$  and  $\text{Co}_{20}\text{Mn}_1$  compared with pure  $\text{Co}_3\text{O}_4$

Table S2 Crystallite sizes of the catalysts before and after the reaction, as estimated from the XRD analysis

Fig. S1 X-ray diffraction patterns of  $\text{Co}_{20}\text{Mn}_1$  before and after exposure to the catalytic  $\text{O}_2$  and  $\text{CH}_4$  reaction.

Fig. S2 X-ray diffraction patterns of  $\text{Cu}/\text{Al}_2\text{O}_3$  catalysts before exposure to the catalytic  $\text{O}_2$  and  $\text{CH}_4$  reaction.

Fig. S3 X-ray diffraction pattern of the  $\gamma\text{-Al}_2\text{O}_3$  used as the Cu-based catalyst support.

Fig. S4 Exemplary in-situ gas analysis showing that no  $\text{H}_2$  production was detected by the RGA under various operating temperature conditions.

**Table S1** XRD peak shifts for  $\text{Co}_{40}\text{Mn}_1$  and  $\text{Co}_{20}\text{Mn}_1$  compared with pure  $\text{Co}_3\text{O}_4$ 

Peak of $\text{Co}_3\text{O}_4$	Before reaction		After reaction	
	$2\theta = 36.8^\circ$	$2\theta = 65.2^\circ$	$2\theta = 36.8^\circ$	$2\theta = 65.2^\circ$
Shift for $\text{Co}_{20}\text{Mn}_1$	$\sim 0.1^\circ$	$\sim 0.2^\circ$	$\sim 0.15^\circ$	$\sim 0.3^\circ$
Shift for $\text{Co}_{40}\text{Mn}_1$	$0^\circ$	$\sim 0.1^\circ$	$\sim 0.1^\circ$	$\sim 0.3^\circ$

**Table S2** Crystallite sizes of the catalysts before and after the reaction, as estimated from the XRD analysis

Catalyst	$\text{Co}_{40}\text{Mn}_1$	$\text{Co}_{20}\text{Mn}_1$	$\text{Cu}20\text{wt\%/Al}_2\text{O}_3$	$\text{Cu}29\text{wt\%/Al}_2\text{O}_3$	$\text{Cu}58\text{wt\%/ZnO-Al}_2\text{O}_3$
Crystallite	$\text{Co}_{3-x}\text{Mn}_x\text{O}_4$	$\text{Co}_{3-x}\text{Mn}_x\text{O}_4$	Cu	Cu	Cu
Crystallite size before reaction, nm	16	15	29	29	26
Crystallite size after reaction, nm	27	28	n.a.	36	n.a.

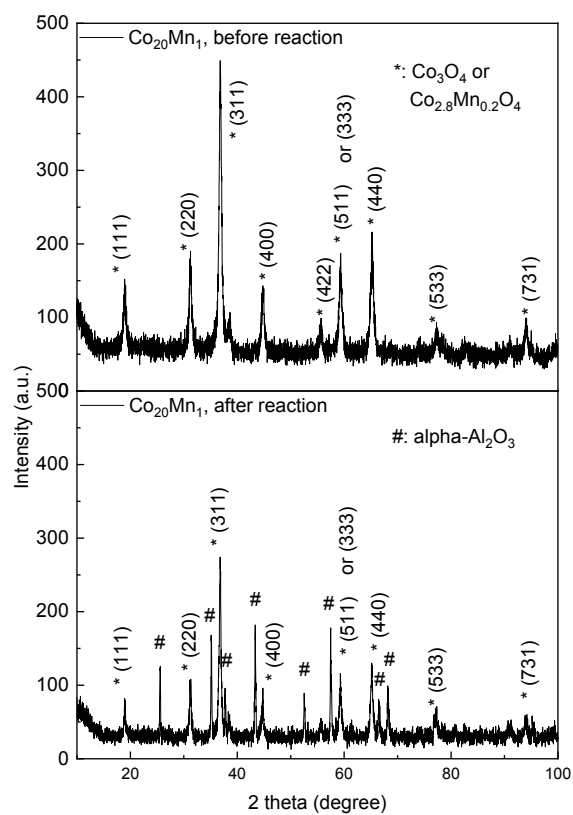


Fig. S1 X-ray diffraction patterns of  $\text{Co}_{20}\text{Mn}_1$  before and after exposure to the catalytic  $\text{O}_2$  and  $\text{CH}_4$  reaction. ( $\alpha\text{-Al}_2\text{O}_3$  detected in the spent catalyst after exposure to the reaction originated from mixing-contamination with heat-trapping alumina beads below and above the catalyst bed.)

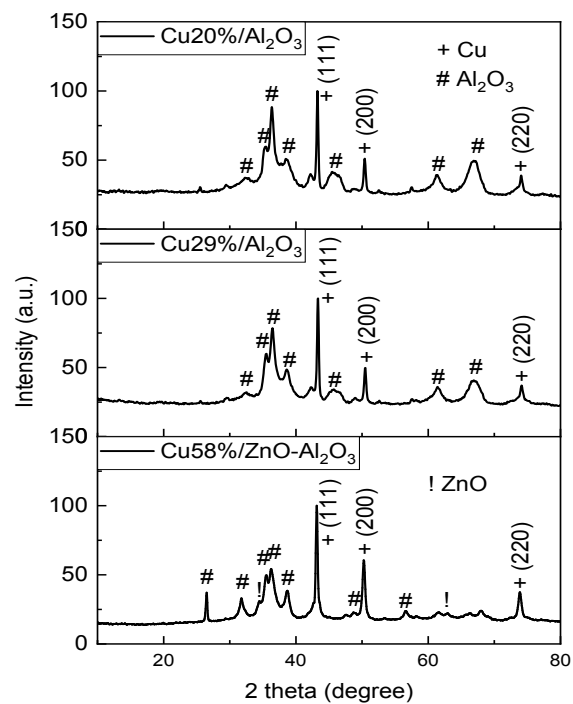


Fig. S2 X-ray diffraction patterns of Cu/Al<sub>2</sub>O<sub>3</sub> catalysts before exposure to the catalytic O<sub>2</sub> and CH<sub>4</sub> reaction.

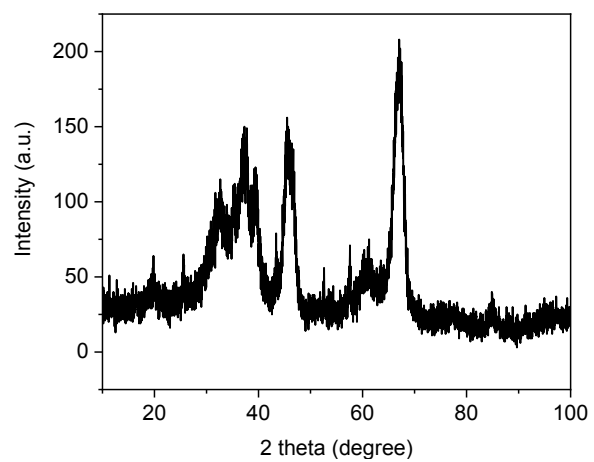


Fig. S3 X-ray diffraction pattern of the  $\gamma$ -Al<sub>2</sub>O<sub>3</sub> used as the Cu-based catalyst support.

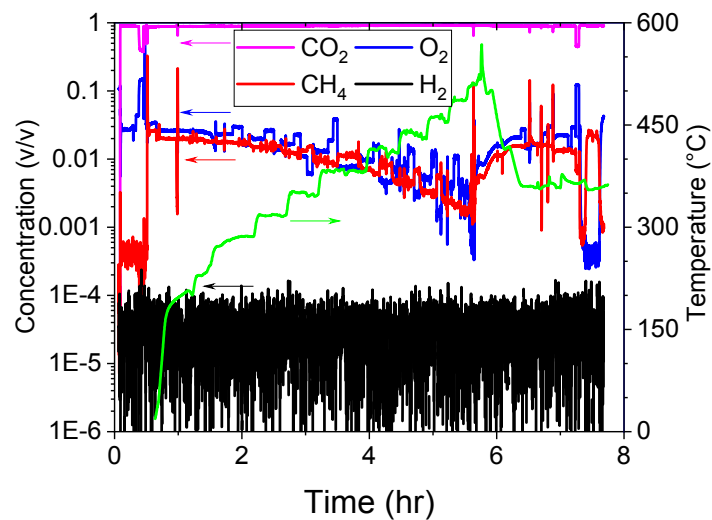


Fig. S4 Exemplary in-situ gas analysis showing that no  $H_2$  production was detected by the RGA under various operating temperature conditions. The concentration of  $H_2$  detected by the RGA in the initial 30 min without any  $CH_4$  injection represented the background noise of the RGA. (Catalyst:  $Co_{40}Mn_1$ ; Gas feed: 1.5–3.75%  $O_2$ , 1.2–2.0%  $CH_4$  and balance  $CO_2$ ; GHSV:  $18,000\text{ h}^{-1}$ ; Flow pattern: one-direction flow)